Bull. Mater. Sci., Vol. 37, No. 3, May 2014, pp. 695–703. © Indian Academy of Sciences.

Processing and characterization of alumina/LAS bioceramics for dental applications

M GUEDES[1,4,*], V COSTA[2], T SILVA[2], A TELES[2], X YANG[2] and A C FERRO[3,4]

[1]Department of Mechanical Engineering, Escola Superior de Tecnologia, Instituto Politécnico de Setúbal, 2910-761 Setúbal, Portugal
[2]Escola Superior de Tecnologia, Instituto Politécnico de Setúbal, 2910-761 Setúbal, Portugal
[3]Department of Mechanical Engineering, Instituto Superior Técnico, TU Lisbon, Av. Rovisco Pais, 1049001 Lisboa, Portugal
[4]ICEMS, Instituto Superior Técnico, TU Lisbon, Av. Rovisco Pais, 1049001 Lisboa, Portugal

MS received 30 December 2012; revised 15 April 213

Abstract. Alumina allows to recreate the functionality and aesthetics of natural teeth. However, its low fracture toughness rises concern regarding use in dental restoration. Structural reliability is addressed here by formulating a material containing alumina and a glass–ceramic from LAS system. The presence of LAS in the mixtures result in formation of glass phase during sintering, promoting densification at lower temperature and enhanced surface finishing. A composite microstructure with increased toughness can thus be produced. Powder mixtures containing 0, 20, 50, 80 and 100 wt%-LAS were prepared by planetary milling and uniaxial pressing and sintered. The compositions were investigated regarding their processability, mechanical performance and biological behaviour. Aesthetics was evaluated by comparison with a commercial dental matching guide. Variations on hardness and fracture toughness with starting LAS fraction were assessed by indentation. Interaction with biological medium was evaluated by immersion in a simulated body fluid. Resulting microstructures were characterised by FEG–SEM, EDS and XRD.

Keywords. Dental materials; alumina; aluminosilicates; LAS glass-ceramics; indentation toughness; biological stability.

1. Introduction

The market for new dental biomaterials is steadily expanding, reflecting not only the need for increasingly reliable materials, but also the growing demand for improved aesthetical appearance. Ceramic materials offer the possibility to recreate the functionality and aesthetics of natural teeth, and are in growing demand for dental restorations ranging from inlays and veneers to dental crowns, bridges and implants. Although ceramics are widely used as dental restorative materials and dental implants, they are typically brittle and present low fracture toughness, which decreases their mechanical reliability. Replacement of failed dental materials imposes unnecessary costs, consumes clinical hours and causes biological damage to the teeth (Stumpf *et al* 2009). Development of new highly reliable and cost-effective bioceramics is thus of great significance to the dentistry community.

The use of medical grade alumina in dental implantology (mainly screws, anchorage elements, pin implants and crowns) was initiated in 1970s (Willmann 1996; Galindo *et al* 2011). Alumina's success is based on the combination of appropriate aesthetic properties, chemical and biological inertness, high mechanical wear resistance, and overall long term stability (Willmann 1996; Fischer *et al* 2008; Stumpf *et al* 2009). Its major drawback concerns brittleness and low fracture toughness with corresponding decreased reliability. The loss of mechanical resistance results from stress concentration around pre-existing structural defects such as pores, flaws and cracks, and are enhanced by the cyclic stress and residual tension that dental ceramics are subjected to the chemical and thermal aggressive environment of the oral cavity (Stumpf *et al* 2009; Borba *et al* 2011). As in any other ceramic material, strengthening of alumina is accomplished through the decrease of the defect population, increase in homogeneity and general improvement of the microstructure (Stumpf *et al* 2009). In this work, the development of tougher alumina dental ceramics is endeavoured through microstructural control by combination with a glass–ceramic, introduced in the glass form at room temperature. During heating of the mixture the glass phase is expected to promote viscous sintering of the powders, with elimination of the pore structure and improvement

*Author for correspondence (mafalda.guedes@estsetubal.ips.pt)

of surface condition. Crystallization of the glass phase eventually takes place, rendering a fine grained structure amid the alumina particles, and thus contributing to increased mechanical properties.

Li_2O–Al_2O_3–SiO_2 (LAS) glass–ceramic system was chosen due to its excellent thermal shock resistance and chemical durability (Hu *et al* 2005) and good mechanical properties (McMillan 1964). In particular, the commercial LAS composition Ceran was used because it had been previously studied by the authors regarding its processing features and potential for fabrication of glass–ceramic matrix composites by the powder route (Guedes *et al* 2001). Crystallization and sintering behaviour as well as the final properties of glass–ceramic parts are affected by the composition of the parent glass, the nucleating system and crystallisation conditions. Therefore, the use of a successfully processed commercial LAS composition minimises the number of experimental parameters. In that work nucleation and crystal growth conditions for Ceran were established by thermal analysis, rendering that surface and volume crystallization take place simultaneously. DTA curves surveyed at 10 °C/min exhibit glass transition temperature at 695 °C and crystallization onset at 871 °C. Two exothermic peaks with maximum at ~ 896 °C and 1077 °C are present and correspond respectively to crystallization from the glass (with formation of β-quartz s.s.) and phase transformation (into β-spodumene and SiO_2); one unidentified crystalline phase was also found at both temperatures. It was also assessed that the sinterability range for Ceran powders is narrow (770–893 °C), showing that sintering is only partial before crystallization begins, because the resulting viscosity increase hinders on full densification by viscous flow.

2. Experimental

Experiments were carried out with CT-1200-SG alumina from ALMATIS (maximum 0·34 wt% impurities according to the manufacturer) (table 1 and figure 1), and the commercial LAS glass–ceramic Ceran from SCHOTT. The glass-ceramic is composed by a large number of oxides (table 2), each one performing a specific function; such a complex composition is common in commercial glass–ceramics (McMillan 1964). LAS glass in frit form (figure 2) was produced by conventional melt-quenching as described elsewhere (Guedes *et al* 2001). Measured particle size and distribution (L1064, CILAS) for both starting powders are shown in table 3.

Homogeneous feedstock of tailored compositions were attained by planetary ball milling (PM100, RETSCH) the appropriate ratios of alumina and LAS glass (table 4) at 400 rpm for 120 min, in the presence of the same weight of water. The fragmented powders were further submitted to another milling cycle (2 min, 200 rpm) in order to introduce and homogenize a binder agent (3 wt%-DARVAN 811, RTV) destined to assure the green

Table 1. Chemical analysis of alumina powders (reported by supplier).

Impurity	wt%
SiO_2	≤ 0·08
MgO	≤ 0·05–0·1
Fe_2O_3	≤ 0·03
CaO	≤ 0·05
Na_2O_3	≤ 0·08

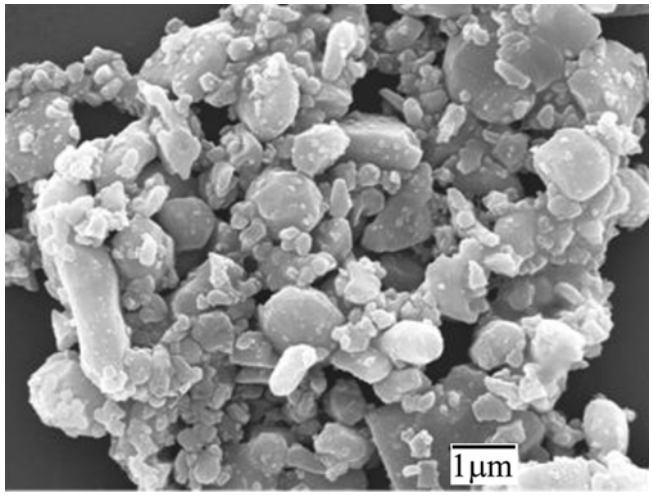

Figure 1. CT–1200–SG alumina particles.

Table 2. Oxides identified in LAS glass in study (Guedes *et al* 2001).

Oxide	wt%	Major function
SiO_2	64·04	Network formers
Al_2O_3	21·34	
Li_2O	3·94	
P_2O_5	0·10	
MgO	0·21	
ZnO	1·24	
TiO_2	2·07	Nucleating agents
ZrO_2	1·66	
Na_2O	1·35	Fluxing agents
BaO	2·28	
CaO	0·08	
MnO	0·21	Colouring agents
NiO	0·35	
CoO	0·26	
Cr_2O_3	0·04	
Fe_2O_3	0·62	
As_2O_3	0·05	Fining agent

Table 3. Particle size distribution in individual powders in study.

	Alumina	LAS
d_{50} (μm)	1·12 ± 0·02	2·80 ± 0·01
Size span	2·15 ± 0·05	1·27 ± 0·05

d: inferior cumulative diameter; size span: width of particle size distribution $(d_{90}–d_{10})/d_{50}$.

strength necessary for handling. The jar's content was oven dried at 40 °C until ~4 wt% incorporated water remained. The resulting powder was separated from the milling balls, screened with cut off size at 600 μm and used in processing dry-pressed bodies. The binder-treated powder mixtures were used to form ceramic discs (ϕ 13 mm) and parallelepipeds (~ 16 × 6 × 6 mm) by uniaxial die pressing (133 MPa, 10 s). The parallelepipeds were used in dilatometric analysis (DI.24, ADAMEL) in order to clarify the samples' densification behaviour and the corresponding sintering onset and completion temperature when heated at 10 °C/min up to 1400 °C. Ceramic discs were used in sintering studies; the samples were heated at 10 °C/min up to the sintering temperature (table 4), followed by 4 h holding time.

Density of green ceramic bodies was measured geometrically; relative density of green compacts was calculated from the rule of mixtures. Absolute and relative density, and total pore fraction and size distribution of fired ceramic bodies were evaluated by mercury intrusion (Autopore IV 9500, Micromeritics).

Microstructural observations were carried out using field emission gun scanning electron microscopy (FEG–SEM) (JSM-7001F, JEOL), coupled with energy dispersive spectroscopy microanalysis (EDS) (Inca pentaFETx3, Oxford Instruments). The crystalline phases presence were assessed by X-ray diffraction analysis (XRD) using CuKα radiation (PW 3020, Philips); samples were scanned in the 2θ range between 10 and 80°, with step size of 0·02° and step time of 2 s.

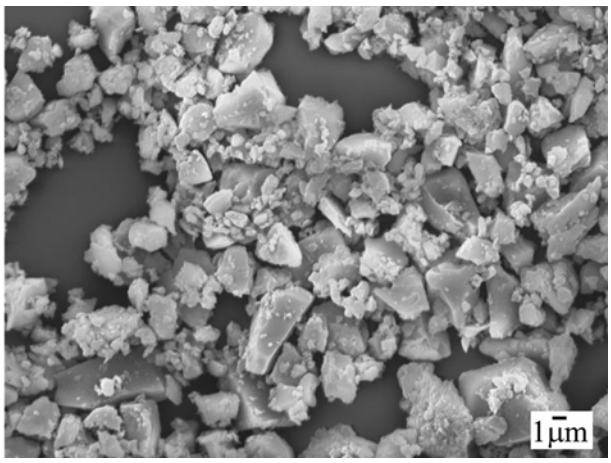

Figure 2. LAS glass frit particles.

Table 4. Alumina/LAS compositions in study and tested sintering temperatures.

Sample designation	LAS : alumina (wt%)	ρ[1] (g/cm^3)	T_s (°C)
0 LAS	0 : 100	3·92	893, 1300
20 LAS	20 : 80	3·54	893, 1150, 1300
50 LAS	50 : 50	3·10	893, 943, 1150, 1300
80 LAS	80 : 20	2·75	893, 1150, 1300
100 LAS	100 : 0	2·56	893, 1150, 1300

ρ, Specific volume; T_s, Sintering temperature.
[1]Theoretical density calculation was based on the rule of mixtures, except for 0 and 100 LAS (density according to the suppliers).

The exposure of the produced alumina/LAS biocomposites to biological environment was tested because, although biomaterials for dental applications must be compatible with the oral environment, bioactivity on the surface of a dental restoration must not occur (ElBatal *et al* 2009). Kokubo and Takadama (2006) established that *in vivo* bioactivity of a material can be evaluated by examining the *in vitro* ability of apatite to form on its surface. Preparation of a simulated body fluid (SBF) and the procedure for apatite-forming ability test followed the protocol developed by the same authors. Unpolished samples of the produced materials were immersed in SBF with ion concentrations similar to those of human blood plasma for four weeks at 36·5 °C (Kokubo and Takadama 2006). The surface of the samples was later examined by EDS in order to detect the presence of elements in solution. At least two samples of each composition (including unmixed LAS) were immersed for reproducibility assessment.

Vickers hardness measurement (30 kgf) was carried out on polished samples using a standard diamond indenter (M4U-025, EMCO), with indentation duration of 10 s. The values of average indentation diagonals were obtained from at least five readings in each sample; the corresponding crack lengths were measured from SEM micrographs. Fracture toughness of sintered materials was estimated using the indentation method by Lawn and Fuller (1975) (1):

$$K_{c,i} = tg\psi \frac{P}{(\pi c)^{3/2}}, \quad (1)$$

where $K_{c,i}$ is the indentation fracture toughness (Pa·m$^{1/2}$), ψ is the half angle of Vickers indenter (i.e. 68°), P is the indentation load (N) and c is the median length (m) of the most severe produced crack in the corresponding indentation mark.

The produced materials were further compared with a teeth shade guide tab (Filtek Z250, 3M) for evaluation of their aesthetical adequacy to dental restoration.

3. Results and discussion

3.1 *Characterization of starting powders*

XRD analysis confirmed that the starting LAS powders are clearly non-crystalline (figure 3). Also, high energy milling does not induce phase transformations upon the studied Al_2O_3–LAS systems: all the crystalline peaks present in the diffractograms after milling correspond to

alumina and are believed to result from contamination from wear of the milling jars. After milling, all powder mixtures show two distinct modes, reflecting both the different volume fraction and the particle size distribution of the starting individual Al_2O_3 and LAS particles. Attained particle size and distribution are shown in table 5. Median particle size varies between ~0·9 μm for unmixed alumina and ~1·5 μm for unmixed LAS, continuously increasing with the amount of LAS present in the powder.

3.2 *Characterization of green bodies*

Particle size distribution reflects upon the attained green density values: wider particle size span corresponds to larger particle size distribution, which in practice leads to better particle packing during powder forming, with improved green density. Accordingly, overall particle size span values accompany the relative density variation, viz. with the broader size span (2·67) corresponding to the denser composition (80 LAS, with ~80% TD), and the narrower size span (2·33) matching the less dense composition (0 LAS, corresponding to ~38% TD of alumina). Depending on the starting LAS amount in the samples, measured density values range from 1·49 g/cm^3 for 0 LAS to 2·40 g/cm^3 for 50 LAS. Both measured density and relative density values are rendered in figure 4.

Dilatometric analysis of pressed samples resulted in sample softening with onset at ~730 °C for 50 LAS samples. This is in fair agreement with previous results reporting Ceran glass transition at 695 °C (Guedes *et al* 2001). Since alumina was added to the base LAS composition, 35 °C difference is attributed to alumina's role as glass network stabilizer, delaying softening onset. Sample softening and attachment to the dilatometer rod prevented continuation of the dilatometric studies and further sintering studies were carried out by trial and error. Glass–ceramic systems sinter by viscous flow of the glass at temperatures above T_g; the sintering process must be preferably within the glass softening range (i.e. between T_g and crystallization onset) (Ferraris and Vernão 1996). A first sintering attempt thus took place at 893 °C, corresponding to sintering completion as determined for unmixed LAS (Guedes *et al* 2001). However, resulting samples are quite fragile and clearly porous and undensified. Additional sinterability runs at 943 °C and 1150 °C revealed the same behaviour, in as much sintering temperature was boosted to 1300 °C.

3.3 *Characterization of sintered bodies*

3.3a *Microstructural characterisation*: After sintering at 1300 °C alumina samples (0 LAS) present 26% porosity: as expected this temperature is not sufficiently high for alumina to achieve full densification in the absence of liquid phase. Although the complete absence of pores are

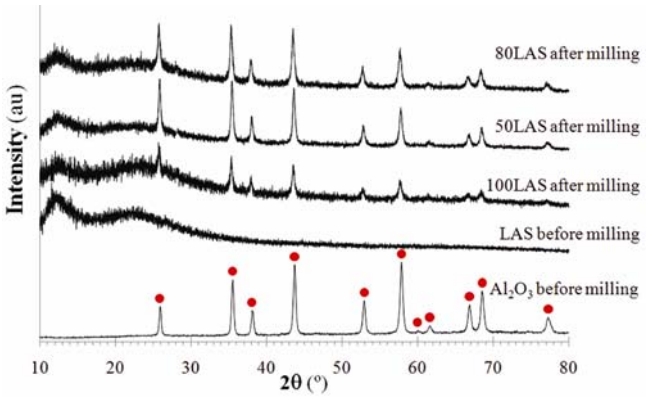

Figure 3. XRD analysis results before and after milling of powder mixtures. All peaks are assigned to Al_2O_3 (●).

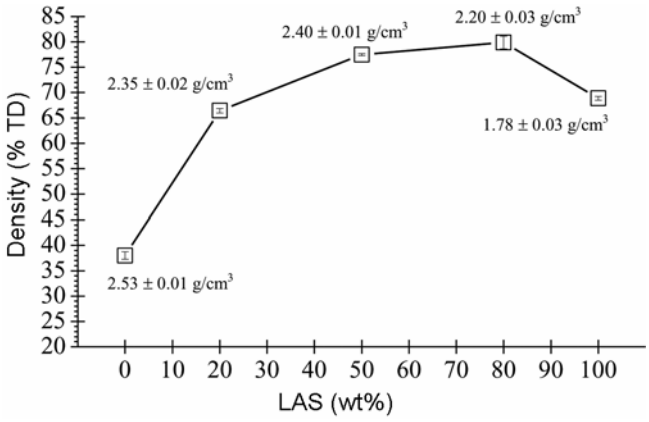

Figure 4. Density of green alumina/LAS samples after pressing as a function of LAS amount. Corresponding geometric density values are shown.

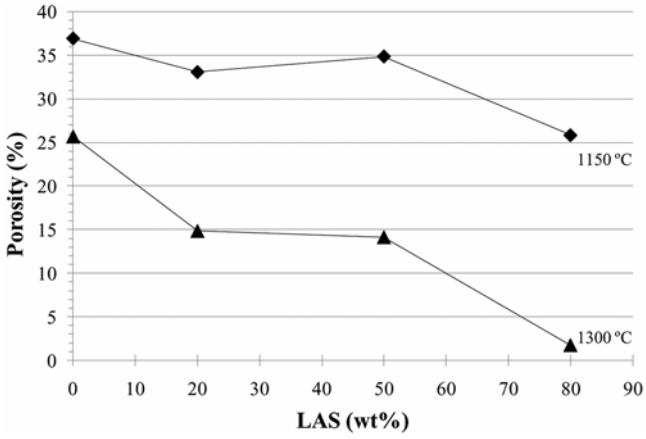

Figure 5. Porosity values for alumina/LAS materials sintered at 1300 °C (▲), as a function of LAS amount. Values attained at 1150 °C (◆) are presented for comparison.

Table 5. Particle size distribution of powder mixtures after milling.

	0LAS	20LAS	50LAS	80LAS	100LAS
d_{50} (μm)	0·88 ± 0·04	0·89 ± 0·02	1·23 ± 0·04	1·23 ± 0·02	1·52 ± 0·11
Size span	2·33 ± 0·21	2·60 ± 0·09	2·60 ± 0·28	2·67 ± 0·10	2·56 ± 0·24

d, Inferior cumulative diameter, size span; width of particle size distribution $(d_{90} - d_{10})/d_{50}$.

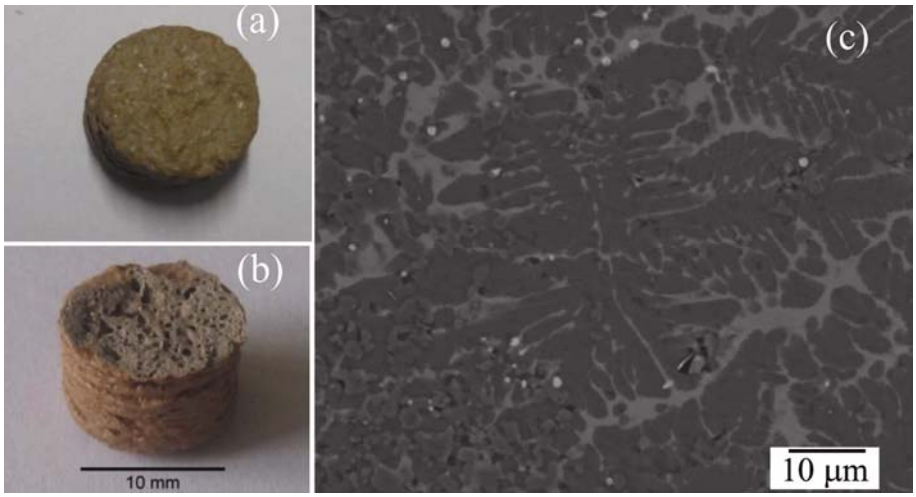

Figure 6. Sample 100 LAS after sintering at 1300 °C: OM image of (**a**) external surface, (**b**) macroscopic porosity and (**c**) BEI image.

a characteristic of glass–ceramics prepared from glass melts (McMillan 1964; Partridge 1994), Al_2O_3/LAS materials produced in the current work via powder route present porosity values between ~ 15% (20 LAS) and 2% (80 LAS) after sintering at 1300 °C (figure 5). 100 LAS composition shows the highest porosity (~ 30%) including internal macroscopic pores (figure 6), which are absent in the other compositions. Porosity does not develop during glass to ceramic conversion, since the overall associated volume changes (which are typically very small in LAS system) result from the production of crystals with different density than the original glass rather than from void formation within the material (McMillan 1964). However, the powder route leads to increased difficulty in achieving full densification, since the large powder's surface area available for nucleation promotes crystallization within each glass particle, resulting in increased viscosity of the system. Therefore, full elimination of the porosity initially present in the green LAS/Al_2O_3 materials was prevented, since both viscous flow of the glass phase and rearrangement of the starting alumina particles within the glass phase are hindered.

It is well known that the properties of glass–ceramic materials are determined by the crystallization phases precipitated from the glass and their microstructures, which depend on composition of the parent glass, thermal treatment and addition of nucleating agents. The heating schedule used in this work did not comprehend a nucleation dwell and crystallization of the glass was not controlled. The fact that Ceran has low activation energy for crystallization (E_a = 196 kJ/mol) and crystal growth index related to simultaneous bulk and surface crystallization (n = 1·5) (Guedes *et al* 2001), ensure a high capability of crystallization. The high imposed temperature rising rate (10 °C/min) was expected to assure that a rigid crystalline skeleton would not form above the nucleation temperature, avoiding hampering viscosity increase. On the other hand, 10 °C/min rate was also expected to be sufficiently low to avoid softening deformation and cracking of the samples. Further, the used sintering temperature (1300 °C) is quite high. At this temperature sufficient energy is supplied to the nucleation and crystallization processes of glass not transformed during heating, provided that a sufficiently long holding time is allowed. Maintenance at 1300 °C assured that satisfactory nucleation and complete crystallization was achieved within 4 h, with only a very small portion of residual glass phase present, viscosity is sufficiently low to allow effective atomic transport. Nucleation and growth were sufficiently slow to allow considerable densification before full crystallization. Within the equipment detection limit, attained XRD data are typical of crystalline materials (figure 7), suggesting that crystallization was almost complete.

In all samples, XRD analysis after sintering at 1300 °C indicates the presence of alumina, silica and a non-stoichiometric aluminosilicate, $Li_xAl_xSi_{3-x}O_6$ (virgilite)

(figure 7). The number and intensity of peaks credited to Al_2O_3 decreases from 20 LAS to 100 LAS sample. This decrease must be not only due to the different starting amount of alumina added to LAS, but also the reaction between Al_2O_3, SiO_2 and Li_2O in the parent glass producing non-stoichiometric aluminosilicate. Accordingly, the aluminosilicate fraction increases from 20 LAS to 100 LAS sample. The number and intensity of peaks credited to SiO_2 increases from 20 LAS to 100 LAS, suggesting silica separation during the crystallization process.

Figure 8 renders the corresponding samples' microstructures. There is no evident relation between particle size and LAS fraction in the starting samples; overall crystal size is in the micron scale. In good agreement with the attained diffractograms, only few silica grains are present in the microstructures. The aluminosilicate phase distribution is intergranular, which suggests that it crystallized from the melt. This phase is thus expected to play a significant role in viscous flow sintering of the materials. The alumina grains, corresponding to the added starting alumina, are slightly more rounded and smoother than the starting alumina particles (figure 1). This suggests some amount of alumina dissolution in the liquid, providing good particle wetting that contributes to pull the grains together by capillary action. Accordingly, the aluminosilicate composition in 80 LAS is richer in Al than any of the other compositions (figure 9), indicating higher interaction between the melt and alumina solid particles. Besides these three crystalline phases identified by XRD, a glass phase is barely visible at the alumina grain boundaries in 20, 50 and 80 LAS materials. This phase is extensively present in 100 LAS material (figures 6(c) and 8(a)), with relative Al : Si : O atomic fraction ratio of 1 : 2·6 : 7 estimated by EDS (figure 9). This chemical composition is similar to the parent LAS glass and also to the aluminosilicate in 100 LAS. These results, together with the visible softening (figure 6(a)) and high porosity (figure 6(b)) of 100 LAS point out the importance of the presence of starting alumina both upon samples porosity, chronology and morphology of phases formed. As a result of its structural role as a glass former, aluminum oxide reduces the tendency of silicate melts to devitrify (McMillan 1964) and shifts parent glass crystallization to higher temperatures (Fernandes *et al* 2010). Also, alumina probably toils as nucleation site for heterogeneous nucleation, favouring crystallization completion. In this way samples 20, 50 and 80 LAS present only residual amount of glass phase and are quite denser than 100 LAS. Full crystallinity of the glass–ceramic in samples with low alumina contents probably require a longer holding period at the crystallization temperature (McMillan 1964).

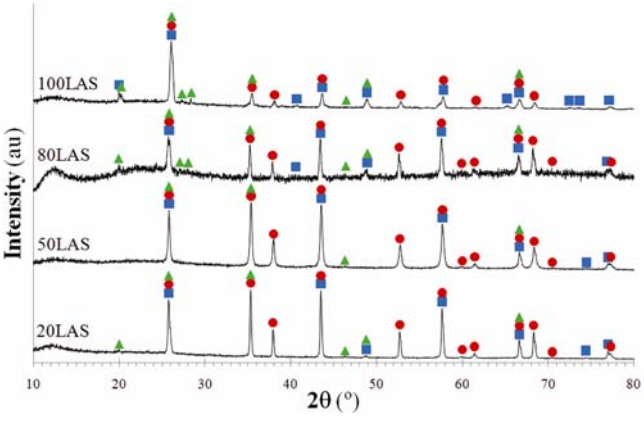

Figure 7. Crystalline phases present in Al_2O_3/LAS materials after sintering at 1300 °C: ● Al_2O_3; ■ $Li_xAl_xSi_{3-x}O_6$ (virgilite); ▲ SiO_2.

Sintered Al_2O_3/LAS materials present skeleton density values of 3·51 ± 0·02 g/cm^3 for 20 LAS, 3·49 ± 0·03 g/cm^3 for 50 LAS and 3·22 ± 0·02 g/cm^3 for 80 LAS.

3.3b *Mechanical characterization*: Attained Vickers hardness results are plotted in figure 10, showing a linear increase in hardness with starting LAS content, ranging from ~ HV525 for 20 LAS to ~ HV1200 for 80 LAS. Apart from the effect of grain size, which does not appear to vary significantly in the sintered samples, the hardness of ceramic materials is also a function of porosity, with monotonic decrease with pore volume fraction increase (Rafferty *et al* 2009). For the compositions studied in this work, the relative density of sintered samples is approximately constant for 20 and 50 LAS, but this difference does not reflect upon the corresponding hardness values. This is probably related to the hardness and fraction of the aluminosilicate phase formed in each of the samples.

Indentation toughness values were determined from radial length of the most severe crack produced during indentation (figure 11) using (2). A linear increase in indentation toughness from ~ 3·6–6·3 MPa·m$^{1/2}$ accompanies the hardness increase with starting LAS fraction in the studied materials (i.e. with porosity decrease).

Observed interaction between cracks and microstructure (figure 12) suggest that the toughening mechanisms responsible for the registered high toughness found in the produced materials are crack deflection and microcracking. The additional work associated with the corresponding crack path diversion and reduction of the crack tip stress concentration factor due to microcracking both contribute to material toughness.

The described hardness and indentation toughness results for the produced biocomposites are summarized and compared with those of natural teeth in table 6. Indentation toughness measurements are much easier to conduct than conventional fracture mechanic techniques, since there is no need for the preparation of specimens with special geometry and complex notches. However, some authors report results for brittle materials in very good agreement with fracture toughness results by

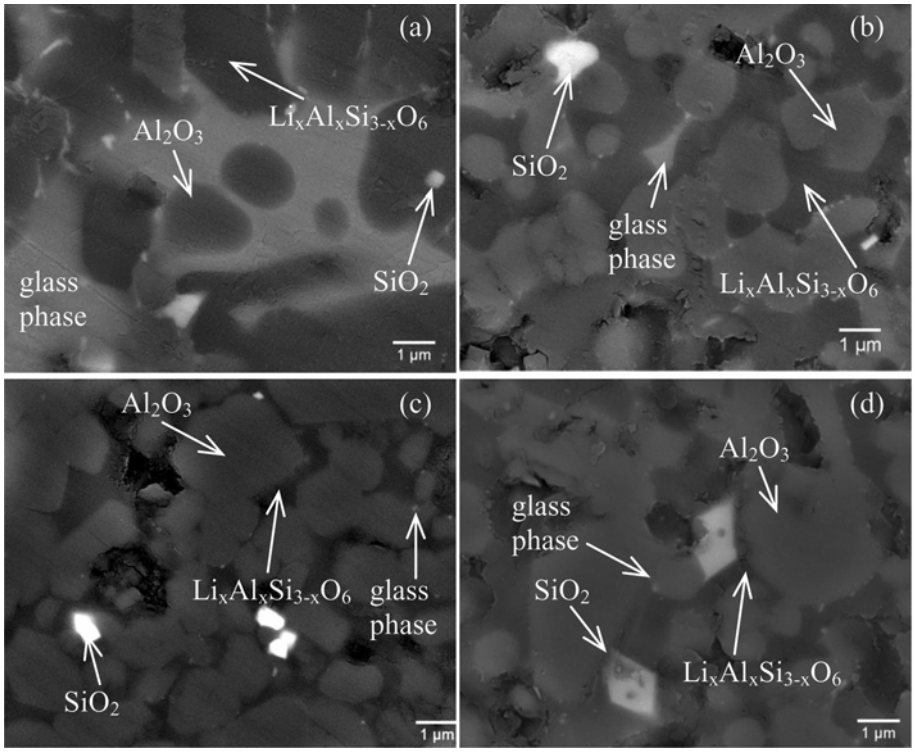

Figure 8. BEI image of Al_2O_3/LAS samples after sintering at 1300 °C: (**a**) 100 LAS; (**b**) 80 LAS; (**c**) 50 LAS and (**d**) 20 LAS.

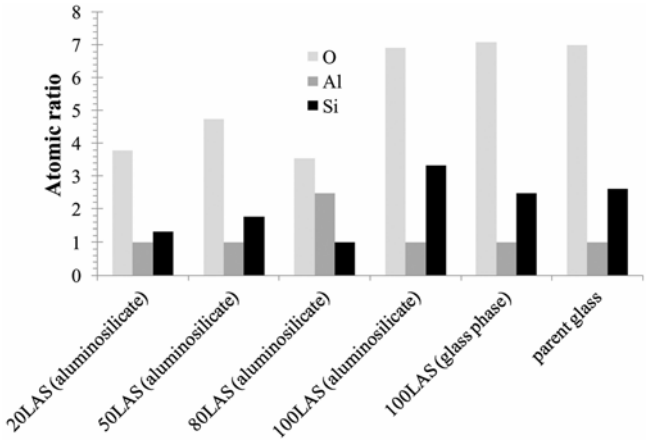

Figure 9. Relative atomic fraction ratio of O (light grey), Al (grey) and Si (black) in microstructural features as a function of LAS composition.

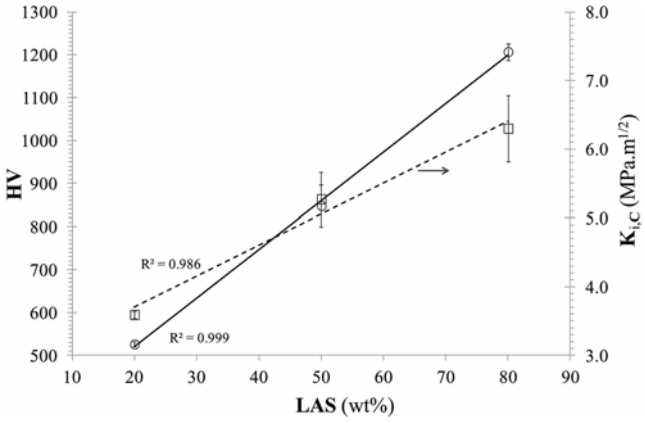

Figure 10. Vickers hardness (○) and indentation toughness (□) results obtained for alumina/LAS materials sintered at 1300 °C as a function of LAS amount.

conventional testing methods, e.g. (Lawn and Fuller 1975; Sergejev and Maksim 2006; Rafferty *et al* 2009), others found consistent higher indentation K_{IC} values (30–48% higher), e.g. (Fischer and Marx 2002). Nevertheless, results found in the current work can be used as a first estimate and are very encouraging regarding the mechanical capability of the developed alumina/LAS materials, especially on what concerns 80 LAS.

3.3c *Assessment of biological stability*: As a consequence of sample exposure to simulated body fluid, it was found that ion deposition leading to formation of apatite (i.e. mainly Ca and P) did not take place. After immersion in SBF for four weeks there was no significant difference between the samples surface microstructure. EDS microanalysis did not reveal the presence of elements other than O, Si and Al on the surface of the samples after immersion. The only exception was trace amounts of sodium, detected on the surface of samples of

Table 6. Mechanical properties of produced biocomposites and of natural teeth. Values for used starting materials are also presented for comparison.

Material	ρ (g/cm^3)	HV	K_C (MPa·m$^{1/2}$)	Reference
Dentine	2·90	46–58	1–3	Zhou and Zheng 2011
Enamel	2·50	239-478	0·7–0·9	Zhou and Zheng 2011
Alumina	3·92	~2000	2–4	Miyayama and Yanagida 1991
Ceran	2·6	~570		Nab *et al* 1995
20 LAS	3·51 ± 0·02	525 ± 12	3·6 ± 0·1	Current work
50 LAS	3·49 ± 0·03	848 ± 98	5·2 ± 0·4	
80 LAS	3·22 ± 0·02	1207 ± 39	6·3 ± 0·5	

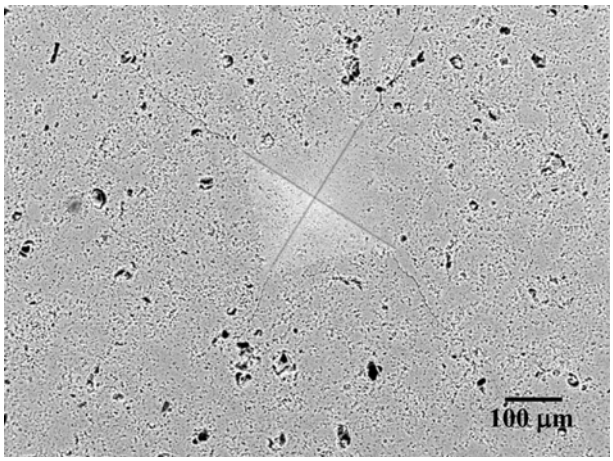

Figure 11. OM image of crack formation from Vickers indentation upon 20 LAS sample.

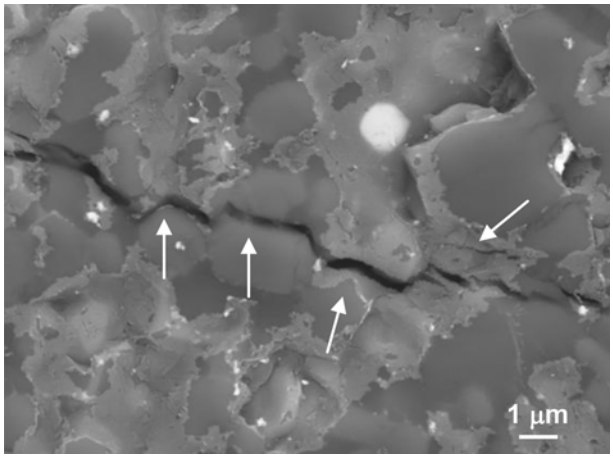

Figure 12. BEI of interaction between advancing cracks and microstructural features in 80 LAS sample showing crack deflection and microcracking (arrows).

all compositions in study (table 7). Sodium is present both in the used distilled water and in reagents for SBF preparation. Sodium deposition upon alumina/LAS samples surface is suggested to result from the high affinity between sodium and alumina (Tel'nova and Grabis 2006). Accordingly, the higher alumina contents in the samples, higher the amount of sodium deposition.

Table 7. Sodium contents on surface of alumina/LAS samples, after immersion in SBF for four weeks.

Material	Surface Na (at%)
20 LAS	0·60 ± 0·01
50 LAS	0·53 ± 0·09
80 LAS	0·27 ± 0·05
100 LAS	0·17 ± 0·03

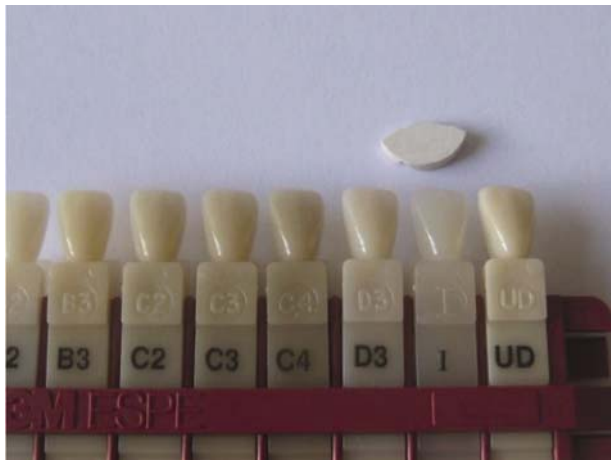

Figure 13. Comparison between 80 LAS and 3 M Filtek shade guide.

The described results suggest that the alumina/LAS materials in study are not bioactive (Kokubo and Takadama 2006). Hence, under the biological stability perspective, the materials are compatible with the oral environment and appropriate for dental applications.

3.3d *Aesthetic evaluation*: Reproduction of the visible appearance of natural teeth (including colour, translucency and fluorescence properties) is a mandatory parameter in the development of materials for dental restoration. Attained materials were compared with a 3 M teeth shade chart (Filtek Z250) for aesthetic classification. The colour of the attained 80 LAS material corresponds to *I* classification in the used shade guide (figure

13). However, its appearance is dull and matte. The material must be additionally veneered with an appropriate dental coating to reproduce more closely the optical properties of natural teeth regarding shimmer and translucency.

It should be mentioned that the starting commercial glass–ceramic Ceran contains a high amount of colourants (transition metal oxides), which affect the aesthetical properties of the produced composite. Some of the oxides present, such as P_2O_5 are known to produce inadequate colours to match the appearance of human teeth; also NiO, TiO_2 and Fe_2O_3 affect the dental material shade and need to be balanced carefully (Anusavice *et al* 1994).

4. Conclusions

Addition of LAS glass to alumina allows the production of composites ceramic/glass–ceramic with encouraging properties regarding the use as dental materials. The most promising composition is a mixture of 20 wt%–alumina/ 80 wt%–LAS. After sintering at 1300 °C for 4 h, this material presents hardness value superior to that of natural teeth and indentation fracture toughness well above that of alumina. Also, the material is biocompatible and presents a colour shade compatible with that of natural teeth, although veneering is in order to reproduce shimmer and translucency.

References

Anusavice K J, Zhang N Z and Moorhead J E 1994 *Dent. Mater.* **10** 141

Borba M, Araújo M D, Fukushima K A, Yoshimura H N, Cesar P F, Griggs J A and Della Bona A 2011 *Dent. Mater.* **27** 710

ElBatal F H, Azooz M A and Hamdy Y M 2009 *Ceram. Int.* **35** 1211

Fernandes H R, Tulyaganov D U, Goel A, Ribeiro M J, Pascual M J and Ferreira J M F 2010 *J. Eur. Ceram. Soc.* **30** 2017

Ferraris M and Vernão E 1996 *J. Eur. Ceram. Soc.* **16** 421

Fischer H and Marx R 2002 *Dent. Mater.* **18** 12

Fischer H, Weiß R and Telle R 2008 *Dent. Mater.* **24** 328

Galindo M L, Sendi P and Marinello C P 2011 *J. Prosthet. Dent.* **106** 23

Guedes M, Ferro A C and Ferreira J M F 2001 *J. Eur. Ceram. Soc.* **21** 1187

Hu A M, Li M, Dali D L, Mao and Liang K M 2005 *Thermochim. Acta* **437** 110

Kokubo T and Takadama H 2006 *Biomaterials* **27** 2907

Lawn B R and Fuller E R 1975 *J. Mater. Sci.* **10** 2016

McMillan P W 1964 *Glass-ceramics* (London: Academic Press)

Miyayama M K and Yanagida Y 1991 *Engineered materials handbook, vol. 4: ceramics and glasses* (ed.) S J Schneider (Ohio: ASM) pp 748–757

Nab P, Rodek E W, Schildt H and Weinberg W 1995 *Low thermal expansion glass ceramics* (ed.) H Bach (Berlin: Springer-Verlag) pp 60–78

Partridge G 1994 *Glass Tech.* **35** 116

Rafferty A, Alsebaie A M, Olabi A G and Prescott T 2009 *J. Colloid Interf. Sci.* **329** 310

Sergejev F and Maksim A 2006 *Proc. Estonian Acad. Sci. Eng.* **12** 388

Stumpf A S G, Bergmann C P, Vicenzi J, Fetter R and Mundstock K S 2009 *Mater. Des.* **30** 4348

Tel'nova G and Grabis Y 2006 *Inorg. Mater.* **42** 50

Willmann G 1996 *J. Mater. Process. Technol.* **56** 168

Zhou Z R and Zheng J 2011 *J. Phys.* **D41** 113001